This is the accepted manuscript version of the contribution published as:

Klünemann, T., Preuß, A., Adamczack, J., **Rosa, L.F.M.**, **Harnisch, F.**, Layer, G., Blankenfeldt, W. (2019):
Crystal structure of dihydro-heme d_1 dehydrogenase NirN from *Pseudomonas aeruginosa* reveals amino acid residues essential for catalysis
J. Mol. Biol. **431** (17), 3246 - 3260

The publisher's version is available at:

http://dx.doi.org/10.1016/j.jmb.2019.05.046

Crystal structure of dihydro-heme d_1 dehydrogenase NirN from *Pseudomonas aeruginosa* reveals amino acid residues essential for catalysis*

Thomas Klünemann[a], Arne Preuß[b], Julia Adamczack[b], Luis F.M. Rosa[c], Falk Harnisch[c], Gunhild Layer[b,d] and Wulf Blankenfeldt[a,e]

[a]Department of Structure and Function of Proteins, Helmholtz Centre for Infection Research, Inhoffenstrasse 7, 38124 Braunschweig, Germany

[b]Institute of Biochemistry, Leipzig University, Brüderstrasse 34, 04103 Leipzig, Germany

[c]Department of Environmental Microbiology, Helmholtz Centre for Environmental Research, Permoserstrasse 15, 04318 Leipzig, Germany

[d]Institute of Pharmaceutical Sciences, University of Freiburg, Stefan-Meier-Str.19, 79104 Freiburg, Germany

[e]Institute for Biochemistry, Biotechnology and Bioinformatics, Technische Universität Braunschweig, 38106 Braunschweig, Germany

Corresponding authors:

Wulf Blankenfeldt, Department of Structure and Function of Proteins, Helmholtz Centre for Infection Research, Inhoffenstrasse 7, 38124 Braunschweig, Germany, Phone: +49 531 6181-7000, Email: wulf.blankenfeldt@helmholtz-hzi.de

Gunhild Layer, Institute of Pharmaceutical Sciences, University of Freiburg, Stefan-Meier-Strasse 19, 79104 Freiburg, Germany, Phone: +49 761 203-8373, Email: gunhild.layer@pharmazie.uni-freiburg.de

Abstract

Many bacteria can switch from oxygen to nitrogen oxides, such as nitrate or nitrite, as terminal electron acceptors in their respiratory chain. This process is called 'denitrification' and enables biofilm formation of the opportunistic human pathogen *Pseudomonas aeruginosa*, making it more resilient to antibiotics and highly adaptable to different habitats. The reduction of nitrite to nitric oxide is a crucial step during denitrification. It is catalyzed by the homodimeric cytochrome cd_1 nitrite reductase (NirS), which utilizes the unique isobacteriochlorin heme d_1 as its reaction center. Even though the reaction mechanism of nitrite reduction is well understood, far less is known about the biosynthesis of heme d_1. The last step of its biosynthesis introduces a double bond in a propionate group of the tetrapyrrole to form an acrylate group. This conversion is catalyzed by the dehydrogenase NirN via a unique reaction mechanism. To get a more detailed insight into this reaction, the crystal structures of NirN with and without bound substrate have been determined. Similar to the homodimeric NirS, the monomeric NirN consists of an eight-bladed heme d_1-binding β-propeller and a cytochrome *c* domain, but their relative orientation differs with respect to NirS. His147 coordinates heme d_1 at the proximal side, whereas His323, which belongs to a flexible loop, binds at the distal position. Tyr461 and His417 are located next to the hydrogen atoms removed during dehydrogenation, suggesting an important role in catalysis. Activity assays with NirN variants revealed the essentiality of His147, His323 and Tyr461, but not of His417.

Keywords

denitrification; heme d_1; NirN; tetrapyrrole biosynthesis; x-ray structure

Abbreviations

CV, cyclic voltammetry; Cyt-c, cytochrome *c*; DHE, d_1-type heme; DT, dithionite; $E^{0'}$, formal potential; NirN, dihydro-heme d_1 dehydrogenase; NirS, cytochrome cd_1 nitrite reductase; PGE, pyrolytic graphite edge-plane; rmsd, root mean square deviation; SHE, standard hydrogen electrode

Introduction

Cytochrome cd_1 nitrite reductase (NirS) is essential for many denitrifying bacteria such as the opportunistic human pathogen *Pseudomonas aeruginosa*[1,2]. During denitrification, nitrite reductase NirS catalyzes the reduction of nitrite (NO_2^-) to nitric oxide (NO)[3,4]. The homodimeric, periplasmic enzyme carries two different tetrapyrrole cofactors, namely a covalently attached heme *c* and a non-covalently bound heme d_1. These cofactors are located in two distinct domains that together build the three-dimensional structure of NirS. Heme *c* is attached to the N-terminal cytochrome *c* domain *via* the cysteine residues of the characteristic CxxCH motif. The isobacteriochlorin heme d_1 (Figure 1) is a unique tetrapyrrole that is bound within a large eight-bladed β-propeller at the C-terminus[5,6]. For nitrite reduction, heme *c* acts as the entry point for the required electron, which is provided by an external electron donor such as the small cytochrome c_{551}[4,7,8]. The electron is then further transferred to heme d_1, at which the reduction of nitrite takes place[9,10]. The produced NO is released upon re-reduction of the heme d_1[11]. The low affinity of NO to ferrous heme d_1 is attributed to its unusual chemical structure, which is not found in any other heme [12]. Due to the combination of methyl and acetate groups at positions C-2 and C-7 and the two unique carbonyl groups at positions C-3 and C-8 of pyrrole rings A and B, heme d_1 possesses the structure of an isobacteriochlorin instead of a porphyrin as found in other hemes. Moreover, heme d_1 carries an acrylate side chain at position C-17 of pyrrole ring D[13]. This acrylate originates from a propionate moiety that is converted into the acrylate group *via* a dehydrogenation reaction, leading to double bond formation (Figure 1). This reaction represents the last step of the heme d_1 biosynthesis pathway, taking place in the periplasm and being catalyzed by the enzyme dihydro-heme d_1 dehydrogenase (NirN)[14]. Recombinant NirN was first purified from the periplasmic protein fraction of *P. aeruginosa* and was shown to be a monomeric *c*-type cytochrome in accordance with its conserved CxxCH motif. However, unlike NirM and NirC,

NirN does not act as an electron acceptor for NirS[15]. Interestingly, the amino acid sequence of NirN exhibits 24% identity to NirS, including significant homology in the heme d_1 binding site. Accordingly, it was demonstrated that NirN from *Paracoccus pantotrophus* binds heme d_1 *in vitro*, utilizing His141 as interaction partner, but is unable to function as a nitrite reductase[16]. At this point, it was still believed that NirN is not involved in heme d_1 biosynthesis, because Δ*nirN* strains from *P. pantotrophus* and *P. aeruginosa* both showed no major growth defect under denitrifying conditions[15,16]. Subsequently, it was shown that NirS from the *P. aeruginosa* Δ*nirN* strain has an altered UV/Vis absorption spectrum, providing a first hint for NirN playing a role in heme d_1 biosynthesis[17]. The physiological role of NirN as the last enzyme of heme d_1 biosynthesis was finally revealed by the isolation of NirS carrying dihydro-heme d_1 from the *P. aeruginosa* Δ*nirN* strain and by an *in vitro* enzyme activity assay showing that purified NirN acts as a dehydrogenase on dihydro-heme d_1[14]. NirN is an unusual dehydrogenase that, unlike other dehydrogenases, does not employ redox cofactors such as FAD or NAD^+ to introduce a double bond in its substrate[14]. Instead, NirN uses the covalently attached heme *c* as the only cofactor required for the conversion of dihydro-heme d_1 into heme d_1[14]. The *in vitro* enzyme activity assay with purified, oxidized (ferric heme *c*) NirN and ferric dihydro-heme d_1 demonstrated that one electron of the two-electron oxidation reaction is transferred to the heme *c* cofactor of NirN, yielding ferrous heme *c*[14]. The second electron remains on the reaction product, which consequently is ferrous heme d_1[14] (Figure 1). For another round of catalysis, the reaction product must be released and heme *c* has to be re-oxidized to the ferric state. The physiological electron acceptor for this regeneration step is currently not known. It is also not known whether the NirN-bound heme d_1 is transferred directly to NirS or if the incorporation of the cofactor into its target enzyme requires other proteins *in vivo*. It was shown that NirN and NirS interact with each other *in vivo*[17], and the transfer of heme d_1 from NirN to NirS was possible *in vitro*[16]. However, many open questions remain. For example,

the active site amino acid residues required for substrate binding and turnover are not known. Therefore, the objectives of this study were (i) to obtain a three-dimensional structure of NirN with and without bound substrate or product in order to identify the active site of the enzyme and (ii) to investigate the function of conserved amino acid residues within the active site.

Results and Discussion

Crystallization of NirN and structure determination

Purified, recombinant NirN from *P. aeruginosa* PAO1 carrying an N-terminal StrepII-tag[14] was crystallized by the sitting drop vapor diffusion method in various polyethylene glycol-containing conditions with poly(*L*-glutamic acid) as a necessary additive. The red NirN crystals diffracted X-rays to a resolution of 1.94 Å. Initial phases were obtained by molecular replacement using the BALBES pipeline[18], which identified the coordinates of NirS (*P. aeruginosa*, PDB ID: 1NIR)[5] as a suitable search model. Two polypeptide chains were placed into the asymmetric unit, corresponding to two independent NirN monomers with an average surface area of 19.4 kÅ^2 as determined by PISA[19]. The monomeric state of NirN found in the crystal is in accordance with the monomeric behavior of NirN in solution that has been described previously[15]. The electron density was sufficient to trace both polypeptide chains and to place one covalently attached heme *c* per chain as well as one molecule of the cryoprotectant (*R*,*R*)-2,3-butandiole at a crystallographic interface. Both chains are nearly identical as judged by the low root mean square deviation (rmsd) of 0.613 Å between C_α positions. Since chain B exhibits a lower overall temperature factor (35.5 Å^2 ± 16.4 Å^2) than chain A (47.5 Å^2 ± 22.0 Å^2), the discussion focusses on chain B except stated otherwise. Data collection and refinement statistics are listed in Supplementary Table 1. Representative electron density maps can be found in Supplementary Figure 1a.

Overall structure

The overall structure of NirN is composed of two distinct domains that are connected by a long linker segment (Figure 2 and Supplementary Figure 2). The N-terminal domain (residues 3-75) harboring the heme *c* cofactor (cyt-*c* domain) possesses an α-helical cytochrome *c* class I fold[20] with axial histidine/methionine coordination of the heme *c* iron ion[20,21]. The cyt-*c* domain sits on top of the larger C-terminal domain (residues 114-468), which exhibits an eight-bladed β-propeller fold and resembles the heme d_1-binding domain of NirS[5,6]. Therefore, we name the C-terminal domain of NirN the "d_1 domain". The linker segment (residues 76-113) connecting the cyt-*c* with the d_1 domain exhibits two loop regions separated by a short α-helix. Overall, the structure of NirN strongly resembles the structure of a NirS subunit with similar domain setup and linker position, as is also confirmed by a search for homologous protein structures within the Protein Data Bank using the DALI server[22]. This search revealed NirS as the closest structural homolog with rmsd values of 2.4 - 3.8 Å and Z-scores in the range of 46.7 - 36.4 depending on the respective NirS structure. However, the relative position of the cyt-*c* domain towards the d_1 domain is unique in NirN and differs from that observed in NirS structures (Figure 3a). The superposition of the NirN structure with the structure of wild type (wt) NirS from *P. aeruginosa* (PDB ID: 1NIR)[5] created by aligning the respective d_1 domains shows that the cyt-*c* domain of NirN is rotated by approx. 60° around an axis parallel to the pseudo-8-fold axis of the β-propeller. A similar rotation of the cytochrome *c* domain relative to the β-propeller was observed in the structures of the NirS variants H327A (PDB ID: 1HZU; Figure 3a) and H369A (PDB ID: 1HZV)[23] from *P. aeruginosa* as well as in structures of NirS from *P. pantotrophus* crystallized under reducing conditions (PDB ID: 1H9X)[24]. In addition to the 60° rotation, the cyt-*c* domain of NirN is also tilted by about 90° when compared to wt NirS. Overall, the described orientation of the cyt-*c* domain in NirN results in a different interaction interface with the d_1 domain than that observed in NirS (discussed in more detail below).

Cytochrome *c* domain

The cyt-*c* domain of NirN adopts a cytochrome *c* class I fold with four α-helices and one 3_{10}-helix (Figure 2 and Supplementary Figures 2 and 3). Heme *c* is covalently attached to the protein *via* thioether linkages with cysteine residues Cys13 and Cys16, and its central iron ion is coordinated by His17 and Met55 (Figure 3b). The coordination by histidine and methionine was already proposed for NirN from *P. pantotrophus* based on amino acid sequence analysis[16]. The heme *c* binding pocket of NirN is mostly hydrophobic (Pro27, Leu29, Leu34, Leu37, Ile46, Phe58, Leu62, Leu70, Leu74) and similar to that of NirS. The propionate side chain of pyrrole ring D of the heme *c* in NirN is involved in polar interactions with residues Arg50, Tyr144 and Arg164, the latter two originating from the d_1 domain (Figure 3b). The propionate carboxylate group of ring C is in contact with His124 *via* a bridging water molecule. These polar interactions of the heme *c* propionate groups are unique for NirN, since the location and orientation of its cyt-*c* domain relative to the d_1 domain is different from the situation in NirS**.**

***d*$_1$ domain**

The d_1 domain of NirN adopts a β-propeller fold with a secondary structure topology strikingly similar to that of the heme d_1-binding domain of NirS (Figure 2 and Supplementary Figure 2 and 3). It consists of eight four-stranded, twisted and antiparallel β-sheets arranged in a circular shape that finishes with a short α-helix at the C-terminus, which partially closes the bottom of the propeller. Except for the first β-sheet, each sheet starts with the N-terminal strand within the propeller and ends with the C-terminal strand at the outer edge. In the case of the first sheet, the innermost strand (β32) belongs to the C-terminus of the protein and the second strand (β1) represents the N-terminus of the d_1 domain. This sheet is the closing point of the propeller and enables the C-terminal α-helix (α6) to partially close the propeller from the bottom. Interestingly, the refined B-factors of the d_1 domain indicate that the second half of the β-propeller is more

flexible than the other (Supplementary Figure 4a). Although this is more significant in chain A, it is present in both chains and may therefore be an inherent property of NirN required for its activity. The long linker segment (residues 76-113) connecting the cyt-*c* with the d_1 domain wraps around the propeller, covering the outer edge of β-sheet 2 and finally merging into strand β1 of the first propeller-sheet (Figure 2 and Supplementary Figure 2 and 3). Overall, the topology, location and conformation of the linker segment of NirN is almost identical to that of NirS.

Domain interface

As described above and illustrated in Figure 2, the cyt-*c* domain sits on top of the d_1 domain where it covers β-sheets 1 and 2 at the upper side of the β-propeller. The propionate side chains of heme *c* point toward the d_1 domain and their carboxylate groups are involved in inter-domain contacts with Tyr144 and Arg164 for the ring D propionate and with His124 (*via* water) for the ring C propionate (see above). As depicted in Figure 3c, several amino acid residues mainly residing on the loops at the top of β-sheets 1, 2 and 3 of the d_1 domain (Arg164, Asp165, Arg183, Leu186 Asn187) establish direct polar contacts or contacts bridged by water with residues on the loop connecting α-helices 2 and 3 of the cyt-*c* domain (Leu22, Thr28, Glu32 and Ser33). Additionally, residues Leu22 and Leu30 of the cyt-*c* domain as well as Leu186 and Leu206 of the d_1 domain together with Pro82 located within the linker segment create a hydrophobic region involving both domains and the linker. The specific hydrophilic and hydrophobic inter-domain interactions stabilize the location and orientation of the cyt-*c* domain relative to the d_1 domain. Most of the amino acid residues participating in inter-domain interactions are at least functionally conserved in NirN proteins from different organisms with exception of Thr28 and Tyr144, the latter being more commonly a phenylalanine (Supplementary Figure 3). Arg164 and Arg183 are strictly conserved in NirN, highlighting their importance for the domain interaction. More thorough analysis utilizing models without the connecting linker revealed that the heme d_1 and cytochrome

c domains in NirN would not form a stable complex according to calculations with PISA[19]. Similar predictions were obtained for NirS. Therefore, it is obvious that the linker is responsible for positioning the cytochrome *c* domain on top of the d_1 domain and for enabling inter-domain flexibility. In case of NirS, this flexibility is considered as part of the reaction cycle[11]. For NirN, only a single domain orientation was observed here, however, other orientations might also be possible.

NirN crystal derivatization

A major aim of this work was to obtain a NirN structure in complex with its substrate or product in order to gather new insights into the active site architecture and the identity of amino acid residues involved in catalysis. Towards this, NirN crystals were soaked in reservoir solution containing either dihydro-heme d_1 (substrate) or heme d_1 (product). During this procedure, the color of the crystals changed from red to green/brown, indicating the binding of the tetrapyrrole. However, for the soaking with heme d_1 the red color was not completely abolished (Supplementary Figure 5). Subsequently, we found a new electron density located inside the ring of the d_1 domain. For maps derived from crystals soaked with dihydro-heme d_1 the electron density was clear enough to place a d_1-type heme in the model (Figure 4a and Supplementary Figure 6). In case of the heme d_1-soaked crystals, the resulting electron density was insufficient to describe the tetrapyrrole completely, probably due to low occupancy of the ligand. Therefore, we chose to only interpret the structure obtained from dihydro-heme d_1-soaked crystals, which could be refined to an R_{work} of 0.192 and an R_{Free} of 0.235 at a resolution of 2.36 Å. Data collection and refinement statistics are listed in Supplementary Table 1 and representative electron density maps can be found in Supplementary Figure 1b. The B-factors of the DHE molecule, which are similar to residues of the low flexible side of the d_1-domain, indicate that the binding site is fully occupied (Supplementary Figure 4b). This was also corroborated by refining DHE at different occupancies.

Here, remaining positive $|F_O-F_C|$ density at occupancy values lower than 0.8 also hinted at a high degree of loading (not shown). Since many enzymes remain active in the crystalline state and NirN crystals were soaked with the substrate dihydro-heme d_1, the bound tetrapyrrole might be either the substrate or the reaction product of NirN, which differ only in the absence or presence of a double bond in the propionate side chain at pyrrole ring D. Due to the moderate resolution it is not possible to clearly distinguish between these two possibilities, and even a mixture of substrate and product might be present. Therefore, we will refer to the bound tetrapyrrole as DHE (for $\underline{d}_1$-type heme) in the following discussion. Despite the unknown reaction state of the NirN/DHE complex, the structural data unequivocally reveal the localization and orientation of the DHE molecule within the active site of NirN and allow the identification of DHE-coordinating amino acid residues.

Structure of NirN in complex with DHE

The DHE molecule binds to the d_1 domain of NirN, where it vertically dives into the upper half of the central, formerly empty cavity of the β-propeller (Figure 4a). The propionate side chains of pyrrole rings C and D point towards the bottom of the d_1 domain, while the carbonyl of ring A and the acetate group of ring B are oriented upwards. The iron-to-iron and edge-to-edge distances between DHE and heme *c* are 23.0 Å and 10.2 Å, respectively. DHE binds to NirN without changing the overall structure or inducing larger conformational rearrangements except for the loop connecting the propeller sheets 5 and 6 (residues 317-327), further referred to as the binding loop (B-loop) here.

Movement of the B-loop

In the structure of NirN without DHE, the central part of the B-loop forms a 3_{10}-helix stabilized from one side through interactions with residues of the loop connecting β-strands 21 and 22 of sheet 6 (Supplementary Figure 7a). Additionally, Ser326 is engaged in a hydrogen bond with the

backbone carbonyl of Phe369, which is part of the loop connecting sheets 6 and 7. From the other side, the B-loop is stabilized by an interaction between the side chain of Asp282 and the backbone amides of His323 and Leu324.

At least two different conformations of the B-loop can be discerned in the NirN/DHE complex. While the first conformation resembles the NirN structure without DHE (Supplementary Figure 7c), the second leads to the formation of a specific ligand recognition motif. In this conformation, Phe369 is pushed towards the protein and consequently loses its contact to Ser326 (Supplementary Figure 7b). The reorientation of Tyr240 towards DHE leads to rearrangement of the hydrophobic interface between β-sheets 4 and 5 (Supplementary Figure 7d) and forces Asp282 to release the B-loop. Together, these local rearrangements lead to a movement of the B-loop that enables His323 to coordinate the central iron ion of DHE and allows Ser326 to form a water-mediated contact to the carboxylate of pyrrole ring D (Supplementary Figure 7b). Notably, both conformations of the B-loop refine to very high but similar B-factors (> 120 $Å^2$) and to comparable occupancy values (chain A, conformation 1/conformation 2: 0.56/0.44; chain B: 0.39/0.61). The high B-factors reflect that this loop is part of the more flexible half of the d_1 domain (Supplemental Figure 4). Remaining unexplained electron density indicates that the two conformations are not sufficient to model the flexibility of the B-loop fully (Supplemental Figure 7e). It is unclear why the B-loop adopts these different conformations despite the fact that the ligand binding site is fully occupied by DHE (see above). Potential explanations include the presence of substrate and product in different oxidation states of the iron cation, which may steer the B-loop towards coordinating the ligand or not.

DHE binding site

The DHE molecule binds to the active site *via* numerous interactions with the surrounding amino acid residues. The central iron ion of DHE is coordinated by the highly conserved His147, which

acts as an axial ligand on one side of the tetrapyrrole. For this, the side chain of His147 swings into the active site by a ~90° -movement compared to its orientation in the NirN structure without DHE (Figure 4c). This histidine has previously been implicated in heme d_1 binding by exchange of the corresponding residue in *P. pantotrophus* NirN (His141) against alanine[16]. The second axial iron ligand is His323 described above. The hydrophobic side of the northern half of DHE (methyl groups of pyrrole rings A and B) is surrounded by a hydrophobic patch composed of amino acid residues Ile343, Phe369, Phe370, Phe385, Leu386 and Trp432, of which Phe369, Phe385 and Leu386 move upon substrate binding in order to accommodate the tetrapyrrole (Figure 4b). The hydrophobic character of this binding patch is conserved in NirN and NirS (Supplementary Figure 3). The polar carboxyl and carbonyl moieties of rings A and B are coordinated by three highly conserved arginine residues and thus experience a positively charged environment (Figure 4c). Arg164, which forms a hydrogen bond with one of the heme *c* carboxylates in the absence of DHE, makes a similar 90° tilting movement towards the ligand as His147 upon substrate binding. In its new position, Arg164 forms hydrogen bonds to the carboxylate groups of pyrrole rings A and B of DHE. For Arg36, which is part of the cytochrome *c* domain, two alternative conformations can be distinguished in the electron density, both different from the one observed in NirN without DHE. In one of these conformations, the guanidinium group stacks with that of Arg164 and in the other it contacts the carbonyl and carboxyl groups of ring A of DHE. Finally, the carbonyl oxygen of ring B in DHE accepts a hydrogen bond from Arg189.

The southern half of DHE perfectly fits into the active site of NirN with almost no adjustments of the interacting residues. The carboxylate group of the ring C propionate moiety is held in position by hydrogen bonds with the side chains of Lys151 and Asn190 as well as with the backbone amide of Gly149 (Figure 4d). Interestingly, Gly148 undergoes a peptide flip upon substrate binding, locating the backbone amide of Gly149 between the carboxyl group of ring C of DHE and the C-

17^1 atom, from which a hydrogen needs to be abstracted during catalysis. This might enable the amide to work as a relay for the carboxyl group to remove a proton from this position. These residues are all strictly conserved in NirN. Tyr240, already mentioned above, completes the environment of the ring C propionate (Figure 4e). The propionate group of pyrrole ring D, which is the site of the dehydrogenation, has a mirrored binding pocket provided by Tyr461, Lys466 and His417 (compared to Tyr240, Lys151 and Asn190, respectively), although the amino group of Lys466 is slightly more distant from the propionate carboxylate of ring D (4.0 Å from Nζ to nearest carboxylate oxygen) than its counterpart of ring C (2.8 Å) (Figure 4d and e). This is compensated by Arg372, which also participates in the coordination of the ring D propionate at a distance of about 3 Å to one of the carboxylate oxygen atoms (Figure 4e). The side chain nitrogen atoms of His417 (Nε) and Asn190 have the same relative position towards the carboxylate of their respective propionate group with a distance to the nearest oxygen of 2.9 Å. As the dehydrogenation reaction is only performed at the propionate side chain of ring D of DHE[14], His417 may directly be involved in catalysis. Additionally, together with Lys466 and Arg372, it provides a positively charged environment for the accommodation of the ring D carboxylate group. Finally, the phenolate oxygen atom of Tyr461 is located at a distance of 3.3 Å from the propionate carbon C-17^2 and at 3.4 Å from C-17^1 (Figure 4d). Thus, Tyr461 might be required for catalysis by abstracting either a proton or a hydrogen atom during the dehydrogenation reaction. All of the described amino acid residues surrounding the ring D propionate are highly conserved in NirN proteins, indicating their importance for substrate binding and/or catalysis.

Comparison of DHE binding in NirN with heme d_1 binding in NirS

The position and orientation of DHE in the NirN/DHE complex are very similar to the position of heme d_1 in structures of NirS. Several amino acid residues involved in tetrapyrrole binding are either identical or functionally conserved. As the overall setup of both enzymes is identical,

differences in the heme d_1 binding site might highlight residues important for NirN function. In the following, the comparison of the binding sites is limited to residues interacting with heme d_1 at the central iron, the propionate side chain of ring D and the oxo-groups of rings A and B (Supplementary Figure 8a, 8b and 3). In NirS, the only axial heme d_1 iron ligand is His182 (*P. aeruginosa* numbering), whereas His369 and His327 are involved in nitrite binding on the opposing side. In NirN, in contrast, two axial ligands (His147, His323) are present, emphasizing that no additional substrates are used in the heme d_1 binding site of this enzyme. The oxo-groups of DHE are coordinated by Arg36 and Arg189 in NirN. In NirS, only the carbonyl of ring B is ligated by Tyr245. The biggest differences between NirN and NirS are found next to the site of propionate dehydrogenation at the D-ring. In NirN, Tyr461 and His417 are close to the hydrogens that are removed during catalysis, whereas the corresponding residues in NirS are the non-reactive Phe533 and Gln483, respectively. In addition, as outlined above, the backbone atoms of Gly148 and Gly149 might be important for NirN function, since these residues reside between both propionates of DHE. In NirS, the backbone of the corresponding residue Ile183 is pushed away from the acrylate as its sidechain is oriented towards heme d_1.

Potential electron tunneling pathway

Due to the different orientations of the cytochrome *c* domains relative to the d_1 domains in NirN and NirS, there are also significant differences in the position of DHE/heme d_1 relative to the respective heme *c* cofactor, yet this results in almost no impact on the heme-to-heme distances (Supplementary Table 2). However, due to the unique domain orientation in NirN, an intriguing connection between the DHE iron ion and the propionate side chains of the heme *c* is established *via* four amino acid residues, namely from His147 to Tyr144. Indeed, calculations done with the PATHWAYS tool[25,26] predict this heme-connecting loop as a likely electron tunneling pathway between the two hemes (Supplemental Figure 8c). The predicted electron jump between Tyr144

and the propionate of heme *c* does not consider the hydroxyl group of tyrosine as part of the pathway, which may explain why the tyrosine is often replaced by a phenylalanine in NirN from other species. The same calculations for NirS from *P. aeruginosa* predict a different electron migration route between heme *c* and heme d_1, connecting them *via* a water molecule and Gly49 and Cys50 of the cytochrome-*c* domain (Supplementary Figure 8d), in line with the different inter-domain orientation in NirS. An identical pathway in NirS was predicted by Wherland *et al*., who utilized a similar calculation method[27].

Redox potentials of dihydro-heme d_1 and heme d_1

Formal potentials ($E^{0'}$) of isolated dihydro-heme d_1 and heme d_1, derived from the oxidation and reduction peak potentials in cyclic voltammetry (CV), were obtained at pH 7.2 using pyrolytic graphite edge-plane (PGE) electrodes, giving values of $E^{0'} = +141$ mV and $E^{0'} = +175$ mV vs. standard hydrogen electrode (SHE) for dihydro-heme d_1 and heme d_1, respectively (Supplementary Figure 9, Supplementary Table 3). The more positive redox potential of heme d_1 ($\Delta E = 34$ mV) implies that the ferrous iron is thermodynamically more stable (lower energy) in heme d_1 than in the precursor molecule, dihydro-heme d_1.

Redox potentials of NirN and NirN-bound heme d_1

CV data for purified NirN was obtained at different pH values (see all raw and analyzed data in Supplementary Figure 10 and Supplementary Table 4). The voltammograms show that NirN (pH 7.2) exhibits two distinct redox peak pairs, one at $E^{0'} = -106$ mV and the second centered at $E^{0'} = +141$ mV. Whereas the signal at higher potential (+141 mV) is attributed to the Met/His-coordinated heme *c* of NirN, the low potential signal (-106 mV) might represent a so-called "Met-loss" conformation. During "Met-loss", the Met-ligand is removed from the iron ion of heme *c*, as previously described for other class I cytochromes *c* and specifically occurs, when these proteins are attached to PGE electrodes[28]. In line with the literature, the potential of the NirN "Met-loss"

state is sensitive to pH changes, as determined within a range of pH 6.0 (-47 mV) to pH 8.2 (-123 mV), while the potential of the Met/His-ligated heme *c* is much less pH-dependent (+156 mV at pH 6.0 and +139 mV at pH 8.2). Redox potentials were also determined after incubating NirN with dihydro-heme d_1 or heme d_1 at pH 7.2. The presence of either tetrapyrrole had no influence on the occurrence of the Met-loss conformation. In the higher potential region, only a single voltammetric wave can be observed at approx. +168 mV for both NirN in the presence of dihydro-heme d_1 or heme d_1 (Supplementary Table 4). In this region, the potentials of heme *c* and substrate or product are too close to be voltammetrically disentangled. However, in both cases the observed $E^{0'}$ is very close to that of heme d_1, suggesting that dihydro-heme d_1 was converted to heme d_1 in the course of the measurement. This is supported by the $E^{0'}$ determined for NirN variant Y461F, which is catalytically inactive (see below). In this case, the high potential signal is detected at about +136 mV both in the presence and absence of dihydro-heme d_1, and this value matches that of heme *c* and that of dihydro-heme d_1. Taken together, the formal potential of the normal Met/His-ligated heme *c* equals that of the substrate dihydro-heme d_1 allowing the electron transfer from the substrate to the cofactor. In contrast, the formal potential of heme d_1 is more positive which is in line with our observation that the reaction product remains in the ferrous state.

Characterization of amino acid residues involved in substrate binding and catalysis

The crystal structure of the NirN/DHE complex revealed the location of the active site and identified amino acid residues involved in DHE coordination. In order to study the importance of selected active site residues in more detail, several single-residue NirN variants were generated. The structural integrity of these variants was confirmed by determination of their melting temperature (Supplementary Table 5) and they were then analyzed for their ability to bind the substrate dihydro-heme d_1 and to catalyze the dehydrogenation reaction. For this purpose, the proteins were mixed with the substrate, and binding as well as reaction progress were followed

under aerobic conditions by UV/Vis absorption spectroscopy (Figures 5 and 6). At the outset of these assays, the heme *c* cofactor was in the oxidized (ferric) state as indicated by a broad absorption band around 528 nm. The unbound dihydro-heme d_1, also in the ferric state, displays a broad absorption band around 671 nm. Upon mixing of wt NirN with the substrate, a new absorption maximum at 610 nm appeared immediately, indicating the binding of dihydro-heme d_1 to the enzyme (Figure 5a). Mixing also starts the reaction, which is evidenced by the immediate emergence of absorption peaks at 522 and 551 nm, representing the reduced (ferrous) heme *c*, and a shoulder around 636 nm, indicative of the formation of ferrous enzyme-bound heme d_1. The traces shown in Fig. 5a indicate that wt NirN completes the reaction within 1 min, but that heme *c* re-oxidizes under the chosen assay conditions (decrease of the peaks at 522 and 551 nm), while the heme d_1 remains in the enzyme-bound ferrous state.

Tyrosine 461 is essential for catalysis

The NirN/DHE complex structure revealed that the sidechain of Tyr461 may be required for hydrogen atom abstraction during the dehydrogenation of dihydro-heme d_1 (Figure 4d). In order to test this hypothesis, Tyr461 was exchanged with phenylalanine. As shown in Figure 5b, the NirN variant Y461F was still able to bind the substrate as judged by the appearance of an absorption band at 610 nm. Despite this, the Y461F variant was completely inactive, since no reduction of the heme *c* and no product formation occurred, indicating that Tyr461 is indeed directly involved in catalysis. The retained ability of NirN Y461F to bind the substrate is in line with the fact that NirS proteins carry a phenylalanine at the corresponding position, where it contributes to the coordination of the acrylate side chain of heme d_1.

Histidine 417 is required for substrate positioning

In addition to Tyr461, His417 is also located in close proximity to the site of dehydrogenation, implicating a role in catalysis and/or substrate binding. Therefore, His417 was exchanged against

alanine or glutamine, but in contrast to Tyr461, this had a less drastic effect on enzyme activity (Figure 5c and d). For the variant H417A, both substrate binding and turnover were slower than for the wt enzyme. In addition, the absorption maximum of the reaction product was observed at 626 nm instead of 636 nm. We suspected that the new absorption band at 626 nm might represent either ferrous heme d_1 released from the enzyme or ferric heme d_1 still bound to NirN[14]. In order to distinguish between these possibilities, the reaction mixture was filtered to separate the enzyme from unbound tetrapyrrole, which revealed that the reaction product was still bound to NirN H417A and not released into the solution. Further, extraction of the reaction product from the enzyme and spectroscopic characterization showed that the product was indeed heme d_1 (Supplementary Figure 12). In order to test whether the enzyme-bound heme d_1 was in the ferric state, the reducing agent dithionite (DT) was added. This, however, did not lead to a significant change in the absorption spectrum, indicating that the reaction product formed by NirN H417A was indeed ferrous heme d_1. A potential reason for the altered absorption spectrum might be changes in the heme d_1 binding mode caused by the amino acid exchange.

Similar effects were observed for the NirN variant H417Q, although not as pronounced as for H417A. In contrast to H417A, the variant H417Q bound the substrate with a similar rate as wt NirN, but the reaction progress was again slower than for the wt enzyme. Further, the reaction product of H417Q displayed an absorption maximum at 631 nm, which is between that observed for H417A and the wt enzyme. Taken together, these results suggest that His417 is required for accurate positioning of the substrate and product, whereas it is not essential for the dehydrogenation reaction.

Histidine 147 is essential for substrate binding

In the NirN/DHE complex, His147 acts as an axial ligand for the central iron ion of DHE. Replacement with alanine or glutamine completely abolished substrate binding and, consequently,

both variants were catalytically inactive (Figure 6a and b). Thus, His147 is essential for substrate binding.

Histidine 323 is involved in substrate binding and positioning

As described above, His323 is located in the flexible B-loop, which can move His323 close to the iron cation of DHE upon binding, such that this residue then may act as the second axial ligand of the substrate. When the respective alanine or glutamine variants were incubated with substrate, the absorption band representing unbound dihydro-heme d_1 at 671 nm disappeared, indicating substrate binding. However, instead of the characteristic absorption band at 610 nm representing the enzyme-bound substrate, we observed a very broad and weak absorption feature around 600 nm and both variants were catalytically inactive (Figure 6c and d). Together, this suggests that His323 indeed acts as an axial iron ligand that might be required for the correct positioning of the substrate within the active site of NirN.

Implications for NirN catalysis

NirN catalyzes the dehydrogenation of a C-C single bond to the corresponding double bond. Usually, such reactions are catalyzed by dehydrogenases that use either a flavin or a nicotinamide as cofactor or cosubstrate acting as electron acceptors. In NirN, however, one of the two electrons lost by the substrate is transferred to the covalently bound heme *c* and the second remains on the central iron ion of the product heme d_1. At present, it is not clear in which form the two hydrogen atoms are removed from the substrate, although a hydride (H^-) transfer seems unlikely due to the lack of a suitable hydride-accepting cofactor. Alternative scenarios involve the abstraction of two protons (2 H^+) or of a single proton (H^+) and a hydrogen atom (H·). The latter alternative would require a radical mechanism.

The structural and functional data presented here reveal that Tyr461 is essential for catalysis, most probably by playing a role in hydrogen removal. It is close enough to both hydrogens to act on

them either as a base or as a radical. Catalytic mechanisms involving tyrosyl radicals are well known (e.g. cyclooxygenases[29] or coproheme decarboxylase HemQ[30]), but it is difficult to envision how such a tyrosyl radical is generated in NirN and how it would be maintained, given that Tyr461 occupies a relatively exposed position. Alternatively, Tyr461 could act as a base to remove at least one of the two protons. Mechanisms involving tyrosinate bases are rare, but known from e.g. alanine racemase[31] or uronic acid-containing polysaccharide lyases[32]. However, similar to the radical mechanism, it is not obvious how the tyrosinate would be generated. Moreover, the pK_a values of the substrate $C17^1$ or $C17^2$ positions are probably much too high for proton abstraction. Because the experiments reported here demonstrate that His417 is not essential for catalysis, only Gly149 remains as another amino acid to play a possible role in the dehydrogenation. The NirN/DHE complex structure suggests that its backbone amide group may function as a proton relay between the propionate sidechain of ring C and the proton at position $C\text{-}17^1$ of the substrate. However, we are unaware of previous instances in which a non-terminal backbone amide has been implicated in enzyme catalysis. Therefore, although Tyr461 was clearly identified as an essential amino acid residue in NirN and Gly149 has an intriguingly interesting position in the NirN/DHE complex, their precise role during catalysis remains to be established in future experiments.

Materials and Methods

Chemicals

All chemicals, media ingredients and other reagents were purchased from Sigma-Aldrich and Carl Roth GmbH & Co. KG unless stated otherwise. Oligonucleotide primers for site directed mutagenesis of the *nirN* gene were obtained from Seqlab Laboratories Göttingen GmbH and are listed in Supplementary Table 6.

Bacterial strains, plasmids and growth conditions

The *Escherichia coli* strains BL21(DE3)[33] and C43(DE3)[34] were used as hosts for recombinant protein production. For plasmid amplification, *E. coli* Stellar™ (Takara), Top10 or XL1-blue were used. *Pseudomonas aeruginosa* PAO1 was used for the production of native $NirS_{WT}$ carrying heme d_1 and the *P. aeruginosa* PAO1 mutant strain RM361 (*nirN::tet*)[35] was used for the production of native $NirS_{\Delta N}$ containing dihydro-heme d_1. *E. coli* strains BL21(DE3) and C43(DE3) were transformed with the plasmids pEC86[36] providing the genes for cytochrome *c* maturation and pET-22b(+)StrepII*nirN*[14] or variations thereof carrying the *nirN* gene (WT or variants) from *P. aeruginosa* PAO1. *E. coli* BL21(DE3) and C43(DE3) carrying both plasmids, pEC86 and pET-22b(+)StrepII*nirN*, were grown in LB-medium supplemented with 100 µg/ml ampicillin and 34 µg/ml chloramphenicol. To support heme *c* production, the medium was further supplemented with 200 µM ammonium ferric citrate or 200µM $Fe(II)SO_4$ and 200 µM 5-aminolevulinic acid (Carbolution Chemicals or Alfa Aesar). The cells were grown at 37°C and 170 r.p.m. to an optical density at 600 nm of 0.6. At this point, recombinant protein production was started by addition of 1 mM IPTG to the medium. The temperature and the revolutions of the shaker were reduced to 20 °C and 120 r.p.m., respectively. The cells were harvested by centrifugation after 24 h. *P. aeruginosa* PAO1 and the *P. aeruginosa* PAO1 mutant strain RM361 were grown under anaerobic conditions in auto-inducer bioassay medium (according to Heydorn *et al.*[37] and further described in Adamczack *et al.*[14]) in sealed bottles with a rubber septum at 37 °C and 140 r.p.m. for 26 h. To support the cofactor synthesis for $NirS_{WT}$ or $NirS_{\Delta N}$, the medium was supplemented with 200 µM ammonium ferric citrate or 200µM $Fe(II)SO_4$ and 200 µM 5-aminolevulinic acid. In all cases, the cells were harvested at 4 °C and the cell pellets were stored at -80 °C.

Mutagenesis of *nirN*

For the generation of derivatives of plasmid pET-22b(+)StrepII*nirN* encoding NirN variants with single amino acid exchanges, the In-Fusion® HD Cloning Kit (Takara) was used according to the manufacturer's instructions. The correct sequence of the *nirN* gene and its variants was verified by DNA sequencing (SeqLab).

Protein purification

Recombinant NirN carrying an N-terminal StrepII-tag was purified using Strep-Tactin Superflow HC resin (IBA GmbH) in gravity flow columns according to the manufacturer's instructions and with 50 mM Tris-HCl (pH 7.5), 150 mM NaCl as the buffer. For protein stability measurements, crystallization experiments and protein film voltammetry, NirN was further purified by size exclusion chromatography using a Superdex 75 10/300 GL column (GE Healthcare) at a flow rate of 0.5 ml/min or a Superdex 75 16/600 column with a flow rate of 1 ml/min and with 50 mM Tris-HCl (pH 7.5), 150 mM NaCl as buffer. Native $NirS_{WT}$ and $NirS_{\Delta N}$ were purified as described previously[14]. Purified proteins were concentrated using VIVA SPIN TURBO filter units (Sartorius AG) and stored at -80 °C until further use.

Extraction of heme d_1 and dihydro-heme d_1 and determination of extinction coefficients

Heme d_1 and dihydro-heme d_1 were extracted from purified $NirS_{WT}$ and $NirS_{\Delta N}$, respectively, as previously described[14]. The dried tetrapyrroles were stored at -80 °C until further use. For the determination of extinction coefficients, the dried tetrapyrroles were dissolved in buffer (50 mM Tris-HCl (pH 7.5), 150 mM NaCl) and UV/Vis absorption spectra were recorded (Shimadzu UV-1650). Then, the iron concentration of the solution, which equals the tetrapyrrole concentration, was determined by inductively coupled plasma mass spectrometry (ICP-MS) (Currenta GmbH, Leverkusen). The determined iron concentrations were used to calculate the extinction coefficient for heme d_1 at 683 nm (ε_{683} = 10.84 mM^{-1} cm^{-1}) and for dihydro-heme d_1 at 670 nm (ε_{670} = 20.53 mM^{-1} cm^{-1}).

NirN activity assay

NirN activity assays were carried out under aerobic conditions at room temperature in a quartz cuvette. 8 µM NirN and 8 µM dihydro-heme d_1 in a total volume of 100 µl of 50 mM Tris-HCl (pH 7.5), 150 mM NaCl were employed. The reaction was started by the addition of the substrate dihydro-heme d_1 to the NirN solution. The reaction progress was followed by recording UV/Vis absorption spectra in the range of 450 -700 nm every 20 s for 5 min using a Shimadzu UV-1650 spectrophotometer and the software UVProbe (Shimadzu).

Cyclic voltammetry

Cyclic voltammetry (CV) was performed by formation of thin films from either concentrated tetrapyrrole solutions, protein solutions or mixtures of both, using a pyrolytic graphite edge-plane (PGE) working electrode (3 mm diameter, 28,27 mm^2 geometric surface area, ALS Co. Ltd., Japan) arranged in a 20 ml three neck-round bottom electrochemical cell using a reference electrode Ag/AgCl (sat. KCl, SE11 Xylem Analytics Germany Sales GmbH & Co. KG, Sensortechnik Meinsberg, Germany) and a 2 cm^2 platinum sheet (99.9 % Pt, GoodFellow, Germany) soldered to a titanium wire as counter electrode. CV was performed using a glavanostat-potentiostat (Bio-logic SP50, Bio-Logic, Claix, France or Palmsens3, Palmsens BV, Netherlands) in either 50 mM HEPES, 100 mM NaCl buffer with pH 7.2 or 8.2, or in 50 mM MES, 100 mM NaCl pH 6.0 buffer. Prior to each experiment, the working electrode surface was polished with 0.3 µm alumina powder on a polishing alumina pad (BASi PK-4 polishing kit, ALS Co. Ltd., Japan), thoroughly washed with water and then incubated for 30 s in an ultrasonic bath. Prior to protein immobilization, the electrode surface was dried with a stream of N_2. Electrode modification was performed by pipetting 4 µl of freshly purified protein or tetrapyrrole solutions (100 µM or higher concentrations) on to the polished electrode, and incubating for 20 s. Excess solution was then removed by rinsing thoroughly with water.

CVs were recorded at a scan rate of 50 mVs^{-1}. For each electrode and conditions, steady state CVs were assured and data was only considered for analysis from the 3rd scan. Capacitive current baseline subtraction was performed using the program SOAS[38]. Determination of peak potentials was done by averaging values of at least 3 independent electrode preparations (i.e. independent replicates – except when noticed). Formal potentials, $E^{0'}$ were calculated from the arithmetic mean of oxidation and reduction peak potentials of the CVs, i.e. midpoint potentials. Error of the average potentials for all measurements was assumed to be within the hardware resolution of the data obtained (± 10 mV).

The measurements for the tetrapyrrole molecules were performed in a closed, N_2 purged electrochemical cell, whereas all the measurements obtained for proteins were performed inside a vinyl anaerobic glove box (Coy, Michigan, USA).

All potentials are provided versus standard hydrogen electrode (SHE) by conversion from Ag/AgCl (sat. KCl; +0.197V vs. SHE).

Determination of melting temperatures

The thermal stability of NirN (wt and variants) was assessed by differential scanning fluorimetry (nanoDSF). The measurements were performed using a Prometheus NT.48 apparatus (NanoTemper Technologies) and the fluorescence emission intensities at 330 nm (F_{330}) and 350 nm (F_{350}) (excitation at 280 nm) between 20-95 °C (ramp 1 °C min^{-1}) were measured. Melting curves were generated by plotting the fluorescence ratios of F_{330}/F_{350} against the temperature. The melting temperature T_m that describes the thermal unfolding transition midpoint was determined by first derivative analysis.

Crystallization of NirN

Crystallization of NirN with N-terminal StrepII-tag was performed by vapor diffusion in sitting drop Intelli 96-3 plates (Art Robbins Instruments). Plates were set up at room temperature with a

HoneyBee 961 crystallization robot (Digilab Genomic Solutions) by mixing 200 nl of an 8.8 mg/ml NirN solution with equal amounts of reservoir solution. The drops were equilibrated against 60 µl of reservoir solution containing 10-14% (w/v) PEG8000 or 11-16% (w/v) PEG3350, 3-7% (w/v) PGA200-400 (Molecular Dimensions) and 0.1 M Tris/HCl pH 7.4-8.0. Crystal growth started between 1 and 5 days and produced mostly crystal clusters or needle bundles as well as individual three-dimensional crystals in some cases, which were used for data collection. For soaking experiments, purified heme d_1 and dihydro-heme d_1 were suspended in the reservoir solution. Both solutions were considered to be saturated with d_1-type hemes as they still contained undissolved green-brown particles, which made a reliable determination of the concentration impossible. In both cases, a concentration above 100 µM can be assumed. The crystals were soaked in this solution for two days. Prior to flash-cooling the crystals in liquid nitrogen, they were cryo-protected by soaking for a few minutes in 9 µl reservoir solution mixed with 1.2 µl (*R*,*R*)-2,3-butanediol.

Data collection, structure determination and refinement

Datasets of NirN crystals and (dihydro)-heme d_1 soaked crystals were collected at the beamline PXIII at the Swiss Light Source (Paul Scherrer Institut, Villigen, Switzerland) on a PILATUS 2M-F detector. All datasets were processed using autoPROC[39] executing POINTLESS[40] and AIMLESS[41] from the CCP4software suite[42] together with XDS[43]. Initial phases were obtained using the molecular replacement pipeline BALBES[18], which found a solution based on the nitrite reductase model 1NIR[5]. Structural models were manually modified using coot (version 0.8.8)[44]. Crystallographic refinement including TLS-refinement and addition of hydrogens in riding positions was performed with phenix.refine[45] of the Phenix suite (version 1.13-2298)[46]. Two conformations of the flexible B-loop (residues 318 – 327) were modeled in the DHE complex. The first conformation was taken from the unliganded structure, the second was build based on

geometric considerations and residual electron density in the vicinity of the iron cation of DHE, which was interpreted as the imidazole moiety of H323. The occupancy of both conformations was set to 50% at the outset of minimization in phenix.refine and then allowed to refine together with B-factors. The PyMOL Molecular Graphics System (Schrödinger LLC; version 1.8.6.2) was used for generating graphical representations of protein structures. Data processing and refinement statistics can be found in Supplementary Table 1.

Accession codes

Coordinates and structure factors for the NirN structure have been deposited in the Protein Data Bank (accession codes: NirN without DHE: 6RTE; NirN with DHE: 6RTD).

References

1. Yamanaka, T., Kijimoto, S., Okunuki, K. & Kusai, K. (1962). Preparation of crystalline *Pseudomonas* cytochrome oxidase and some of its properties. *Nature* **194**, 759–760.
2. Zumft, W. G. (1997). Cell biology and molecular basis of denitrification. *Microbiol Mol Biol Rev* **61**, 533–616.
3. Cutruzzolà, F., Rinaldo, S., Centola, F. & Brunori, M. (2003). NO production by *Pseudomonas aeruginosa cd*$_1$ nitrite reductase. *IUBMB Life* **55**, 617–621.
4. Yamanaka, T., Ota, A. & Okunuki, K. (1961). A nitrite reducing system reconstructed with purified cytochrome components of Pseudomonas aeruginosa. *Biochim Biophys Acta* **53**, 294–308.
5. Nurizzo, D., Silvestrini, M. C., Mathieu, M., Cutruzzolà, F., Bourgeois, D., Fülöp, V. *et al. (*1997). N-terminal arm exchange is observed in the 2.15 A crystal structure of oxidized nitrite reductase from *Pseudomonas aeruginosa*. *Structure* **5**, 1157–1171.
6. Fülöp, V., Moir, J. W., Ferguson, S. J. & Hajdu, J. (1995). The anatomy of a bifunctional enzyme. Structural basis for reduction of oxygen to water and synthesis of nitric oxide by cytochrome *cd*$_1$. *Cell* **81**, 369–377.
7. Silvestrini, M. C., Tordi, M. G., Colosimo, A., Antonini, E. & Brunori, M. (1982). The kinetics of electron transfer between *Pseudomonas aeruginosa* cytochrome *c*-551 and its oxidase. *Biochem J* **203**, 445–451.
8. Vijgenboom, E., Busch, J. E. & Canters, G. W. (1997). *In vivo* studies disprove an obligatory role of azurin in denitrification in *Pseudomonas aeruginosa* and show that azu expression is under control of rpoS and ANR. *Microbiology (Reading, England)* **143 (Pt 9)**, 2853–2863.
9. Farver, O., Brunori, M., Cutruzzolà, F., Rinaldo, S., Wherland, S. & Pecht, I. (2009). Intramolecular electron transfer in *Pseudomonas aeruginosa cd*$_1$ nitrite reductase. Thermodynamics and kinetics. *Biophys J* **96**, 2849–2856.

10. Kobayashi, K., Koppenhöfer, A., Ferguson, S. J. & Tagawa, S. (1997). Pulse radiolysis studies on cytochrome *cd*$_1$ nitrite reductase from *Thiosphaera pantotropha*. Evidence for a fast intramolecular electron transfer from *c*-heme to *d*$_1$-heme. *Biochemistry* **36**, 13611–13616.
11. Rinaldo, S., Sam, K. A., Castiglione, N., Stelitano, V., Arcovito, A., Brunori, M. *et al. (*2011). Observation of fast release of NO from ferrous d_1 haem allows formulation of a unified reaction mechanism for cytochrome cd_1 nitrite reductases. *Biochem J* **435**, 217–225.
12. Allen, J. W. A., Barker, P. D., Daltrop, O., Stevens, J. M., Tomlinson, E. J., Sinha, N. *et al. (*2005). Why isn't 'standard' heme good enough for *c*-type and *d*$_1$-type cytochromes? *Dalton Trans*, 3410–3418.
13. Chang, C. K., Timkovich, R. & Wu, W. (1986). Evidence that heme *d*$_1$ is a 1,3-porphyrindione. *Biochemistry* **25**, 8447–8453.
14. Adamczack, J., Hoffmann, M., Papke, U., Haufschildt, K., Nicke, T., Bröring, M. *et al. (*2014). NirN protein from *Pseudomonas aeruginosa* is a novel electron-bifurcating dehydrogenase catalyzing the last step of heme *d*$_1$ biosynthesis. *J Biol Chem* **289**, 30753–30762.
15. Hasegawa, N., Arai, H. & Igarashi, Y. (2001). Two *c*-type cytochromes, NirM and NirC, encoded in the nir gene cluster of *Pseudomonas aeruginosa* act as electron donors for nitrite reductase. *Biochem Biophys Res Commun* **288**, 1223–1230.
16. Zajicek, R. S., Bali, S., Arnold, S., Brindley, A. A., Warren, M. J. & Ferguson, S. J. (2009). *d*$_1$ haem biogenesis - assessing the roles of three *nir* gene products. *FEBS J* **276**, 6399–6411.
17. Nicke, T., Schnitzer, T., Münch, K., Adamczack, J., Haufschildt, K., Buchmeier, S. *et al. (*2013). Maturation of the cytochrome *cd*$_1$ nitrite reductase NirS from *Pseudomonas aeruginosa* requires transient interactions between the three proteins NirS, NirN and NirF. *Biosci Rep* **33**.
18. Long, F., Vagin, A. A., Young, P. & Murshudov, G. N. (2008). BALBES. A molecular-replacement pipeline. *Acta Crystallogr D Biol Crystallogr* **64**, 125–132.
19. Krissinel, E. & Henrick, K. (2007). Inference of macromolecular assemblies from crystalline state. *J Mol Biol* **372**, 774–797.
20. Almassy, R. J. & Dickerson, R. E. (1978). *Pseudomonas cytochrome c*$_{551}$ at 2.0 A resolution. Enlargement of the cytochrome *c* family. *Proc Natl Acad Sci USA* **75**, 2674–2678.
21. Chothia, C. & Lesk, A. M. (1985). Helix movements and the reconstruction of the haem pocket during the evolution of the cytochrome *c* family. *J Mol Biol* **182**, 151–158.
22. Holm, L. & Laakso, L. M. (2016). Dali server update. *Nucleic Acids Res* **44**, W351-5.
23. Brown, K., Roig-Zamboni, V., Cutruzzolà, F., Arese, M., Sun, W., Brunori, M. *et al. (*2001). Domain swing upon His to Ala mutation in nitrite reductase of *Pseudomonas aeruginosa*. *J Mol Biol* **312**, 541–554.
24. Sjögren, T. & Hajdu, J. (2001). The Structure of an alternative form of Paracoccus pantotrophus cytochrome cd(1) nitrite reductase. *J Biol Chem* **276**, 29450–29455.
25. Humphrey, W., Dalke, A. & Schulten, K. (1996). VMD. Visual molecular dynamics. *J Mol Graph* **14**, 33-8, 27-8.
26. Balabin, I. A., Hu, X. & Beratan, D. N. (2012). Exploring biological electron transfer pathway dynamics with the Pathways plugin for VMD. *J Comput Chem* **33**, 906–910.
27. Wherland, S., Farver, O. & Pecht, I. (2005). Intramolecular electron transfer in nitrite reductases. *ChemPhysChem* **6**, 805–812.
28. Levin, B. D., Walsh, K. A., Sullivan, K. K., Bren, K. L. & Elliott, S. J. (2015). Methionine ligand lability of homologous monoheme cytochromes c. *Inorganic chemistry* **54**, 38–46.
29. Marnett, L. J. (2000). Cyclooxygenase mechanisms. *Current Opinion in Chemical Biology* **4**, 545–552.

30. Celis, A. I., Gauss, G. H., Streit, B. R., Shisler, K., Moraski, G. C., Rodgers, K. R. *et al. (*2017). Structure-Based Mechanism for Oxidative Decarboxylation Reactions Mediated by Amino Acids and Heme Propionates in Coproheme Decarboxylase (HemQ). *J Am Chem Soc* **139**, 1900–1911.
31. Spies, M. A. & Toney, M. D. (2003). Multiple hydrogen kinetic isotope effects for enzymes catalyzing exchange with solvent: application to alanine racemase. *Biochemistry* **42**, 5099–5107.
32. Garron, M.-L. & Cygler, M. (2010). Structural and mechanistic classification of uronic acid-containing polysaccharide lyases. *Glycobiology* **20**, 1547–1573.
33. Studier, F. W. & Moffatt, B. A. (1986). Use of bacteriophage T7 RNA polymerase to direct selective high-level expression of cloned genes. *J Mol Biol* **189**, 113–130.
34. Miroux, B. & Walker, J. E. (1996). Over-production of proteins in *Escherichia coli*. Mutant hosts that allow synthesis of some membrane proteins and globular proteins at high levels. *J Mol Biol* **260**, 289–298.
35. Kawasaki, S., Arai, H., Kodama, T. & Igarashi, Y. (1997). Gene cluster for dissimilatory nitrite reductase (nir) from Pseudomonas aeruginosa: sequencing and identification of a locus for heme d1 biosynthesis. *Journal of bacteriology* **179**, 235–242.
36. Arslan, E., Schulz, H., Zufferey, R., Künzler, P. & Thöny-Meyer, L. (1998). Overproduction of the *Bradyrhizobium japonicum c*-type cytochrome subunits of the cbb_3 oxidase in *Escherichia coli*. *Biochem Biophys Res Commun* **251**, 744–747.
37. Heydorn, A., Nielsen, A. T., Hentzer, M., Sternberg, C., Givskov, M., Ersbøll, B. K. *et al. (*2000). Quantification of biofilm structures by the novel computer program COMSTAT. *Microbiology (Reading, England)* **146 (Pt 10)**, 2395–2407.
38. Fourmond, V., Hoke, K., Heering, H. A., Baffert, C., Leroux, F., Bertrand, P. *et al. (*2009). SOAS: a free program to analyze electrochemical data and other one-dimensional signals. *Bioelectrochemistry (Amsterdam, Netherlands)* **76**, 141–147.
39. Vonrhein, C., Flensburg, C., Keller, P., Sharff, A., Smart, O., Paciorek, W. *et al. (*2011). Data processing and analysis with the autoPROC toolbox. *Acta Crystallogr D Biol Crystallogr* **67**, 293–302.
40. Evans, P. R. & Murshudov, G. N. (2013). How good are my data and what is the resolution? *Acta Crystallogr D Biol Crystallogr* **69**, 1204–1214.
41. Evans, P. (2006). Scaling and assessment of data quality. *Acta Crystallogr D Biol Crystallogr* **62**, 72–82.
42. Winn, M. D., Ballard, C. C., Cowtan, K. D., Dodson, E. J., Emsley, P., Evans, P. R. *et al. (*2011). Overview of the CCP4 suite and current developments. *Acta Crystallogr D Biol Crystallogr* **67**, 235–242.
43. Kabsch, W. (2010). XDS. *Acta Crystallogr D Biol Crystallogr* **66**, 125–132.
44. Emsley, P. & Crispin, M. (2018). Structural analysis of glycoproteins: building N-linked glycans with Coot. *Acta crystallographica. Section D, Structural biology* **74**, 256–263.
45. Afonine, P. V., Grosse-Kunstleve, R. W., Echols, N., Headd, J. J., Moriarty, N. W., Mustyakimov, M. *et al. (*2012). Towards automated crystallographic structure refinement with phenix.refine. *Acta Crystallogr D Biol Crystallogr* **68**, 352–367.
46. Adams, P. D., Afonine, P. V., Bunkóczi, G., Chen, V. B., Davis, I. W., Echols, N. *et al. (*2010). PHENIX: a comprehensive Python-based system for macromolecular structure solution. *Acta Crystallogr D Biol Crystallogr* **66**, 213–221.

Acknowledgements

We thank the MX-Team PXIII at the Swiss Light Source (Paul Scherrer Institut, Villigen, Switzerland) for their beamline assistance. This work was supported by grants from the Deutsche Forschungsgemeinschaft to GL (LA 2412/3-2) and WB (PROCOMPAS graduate school, GRK 2223/1). FH acknowledges support by the BMBF (Research Award "Next generation biotechnological Processes—Biotechnology 2020+") and the Helmholtz-Association (Young Investigators Group). This work was supported by the Helmholtz-Association within the Research Programme Renewable Energies.

Figure Legends

Figure 1: Structures of dihydro-heme d_1 and heme d_1 and the NirN reaction. (a) NirN catalyzes the dehydrogenation of the ring D propionate side chain of dihydro-heme d_1 yielding the acrylate side chain of heme d_1. The numbering of the carbon atoms and the pyrrole rings is indicated for dihydro-heme d_1. The site of dehydrogenation is highlighted in red **(b)** In the *in vitro* enzyme activity assay, the two-electron oxidation of the propionate side chain goes along with the reduction of the heme *c* cofactor and the reaction product heme d_1.

Figure 2: Crystal structure of NirN from *P. aeruginosa*. Cartoon representation of chain B viewed from the side **(a)** and from the top **(b)**. The cyt-*c* domain (residues 3-75) is colored in dark red, the linker section (residues 76-113) in deep-blue and the d1 domain (residues 114-468) in dark-green. Heme *c* is shown as ball-and-stick model and the amino acid residues Cys13, Cys16, His17 and Met55 are depicted as sticks. The protein surface is indicated in light grey.

Figure 3: Domain interface analysis. (a) Top view of NirN, NirS (PDB ID:1NIR) and NirS H327A (PDB ID:1HZU[23]) in cartoon representation depicted from the same point of view after

superposition of the d_1 domains. Note the different domain orientations. Domains of NirN and NirS are colored according to Figure 2. Heme *c* in pink and heme d_1 in cyan are presented as ball and sticks. **(b)** Detailed view of the N-terminal cyt-*c* domain of NirN. The heme *c* is covalently attached to the protein *via* residues Cys13 and Cys16. The axial ligands of the central iron ion are His17 and Met55. The propionate side chains of the heme *c* are coordinated by residues Arg50, Arg164, Tyr144, His124 (*via* water) and several water molecules. Metal-ligand bonds are shown as grey solid lines. **(c)** Detailed view of domain interface of NirN. Interacting amino acids depicted as sticks, water molecules as small spheres and hydrogen bonds indicated as yellow dashed lines.

Figure 4: Crystal structure of the NirN/DHE complex. (a) Overview of NirN with bound DHE depicted as light blue ball and stick model. The blue mesh indicates the $F_{o,soaked}$-$F_{o,unsoaked}$ map calculated utilizing the phases of the NirN structure without bound DHE at a σ-level of 2.5. **(b-e)** Depiction of amino acid residues coordinating DHE. The positions of residues of the superposed NirN structure without DHE are depicted as black lines. Parts of the backbone has been excluded for better visibility of the binding side.

Figure 5: NirN enzyme activity. (a) – (d) UV/Vis absorption spectra recorded during NirN activity assays employing wt NirN (a) and the NirN variants Y461F (b), H417A (c) and H417Q (d). Spectra of the enzyme and the substrate were recorded before mixing (dashed lines) and the progress of the reaction (light grey to black lines) was followed by recording spectra every 20 s for 5 min. Characteristic absorption peaks are labeled.

Figure 6: NirN enzyme activity. (a) – (d) UV/Vis absorption spectra recorded during NirN activity assays employing the NirN variants H147A (a), H147Q (b), H323A (c) and H323Q (d). Spectra of the enzyme and the substrate were recorded before mixing (dashed lines) and the progress of the reaction (light grey to black lines) was followed by recording spectra every 20 s for 5 min. Characteristic absorption peaks are labeled.

Figures

Figure 1

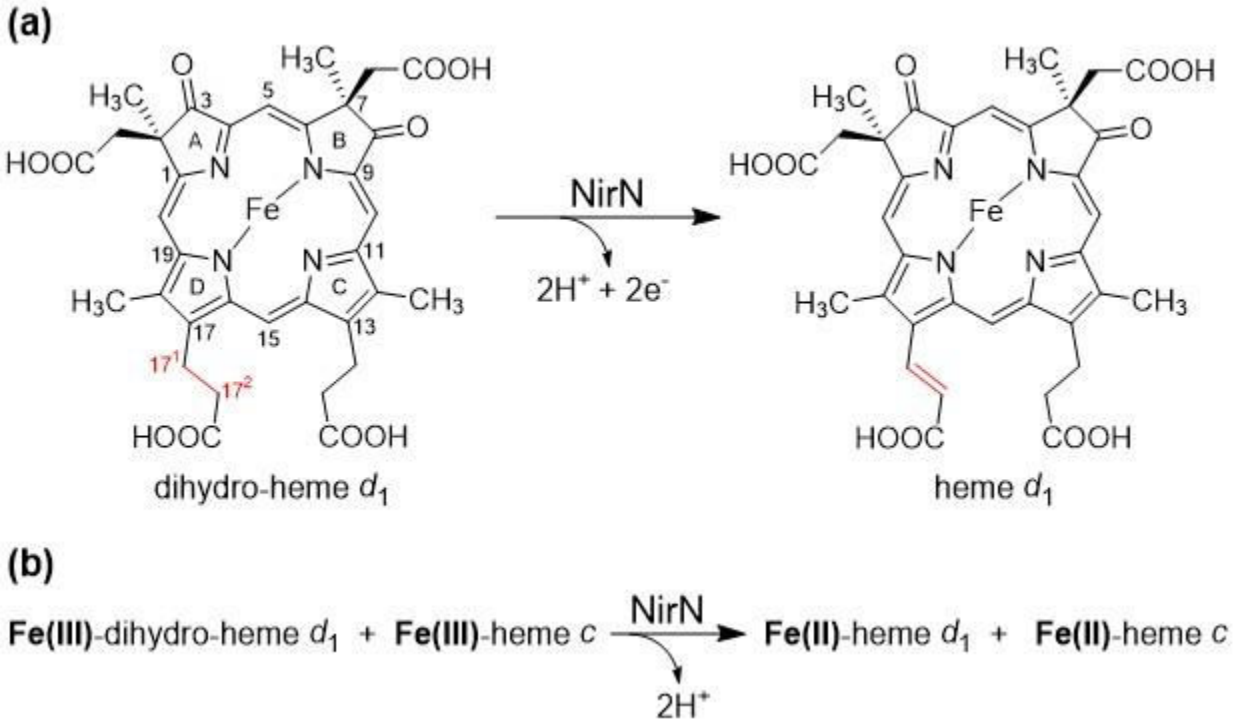

Figure 2

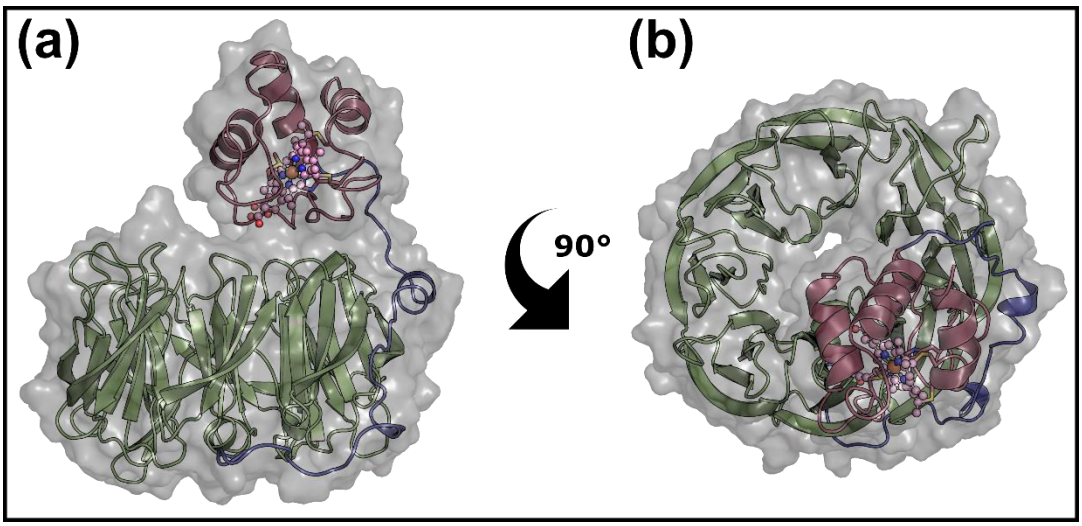

Figure 3

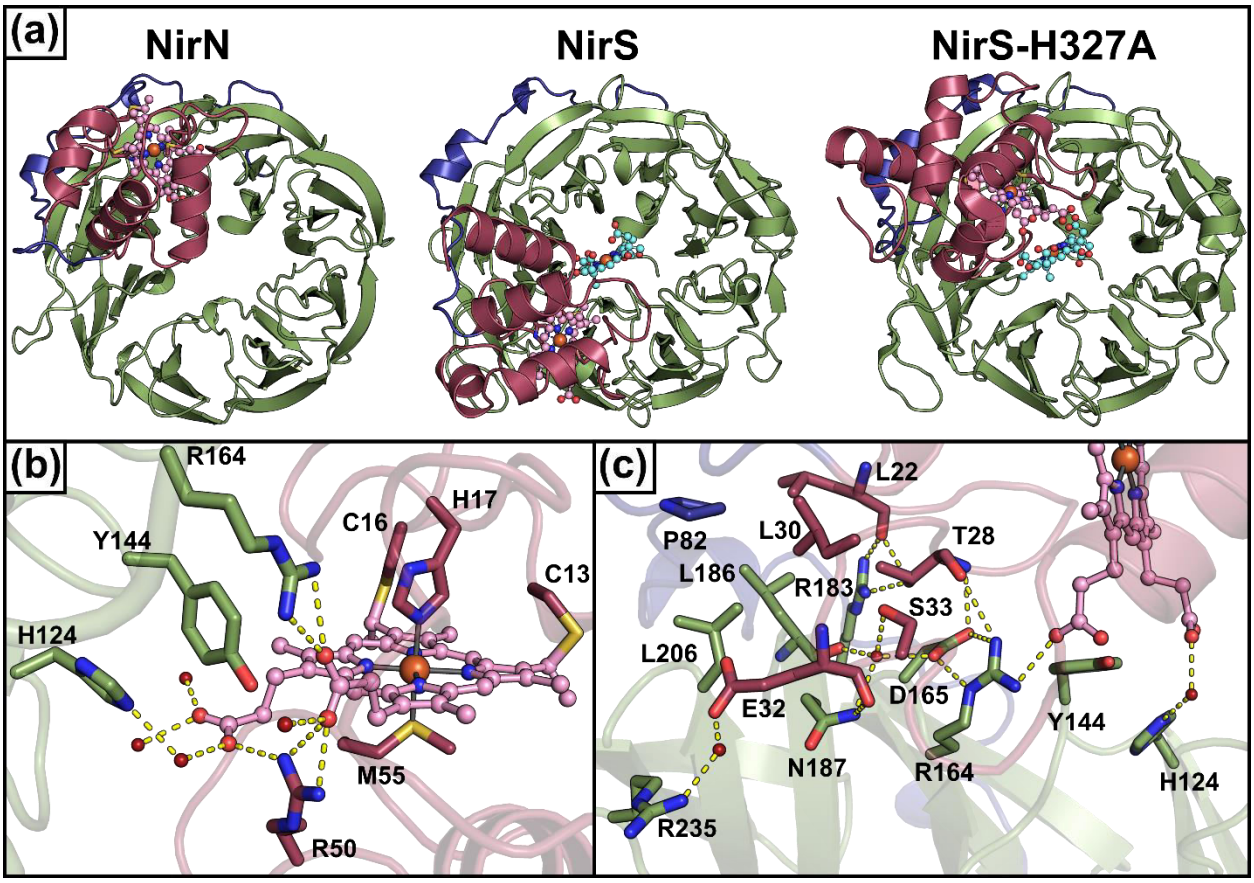
(a)
NirN
NirS
NirS-H327A
(b)
R164
Y144
C16
H17
C13
H124
M55
R50
(c)
L22
P82
L30
T28
L186
R183
S33
L206
E32
D165
Y144
N187
R164
H124
R235

Figure 4

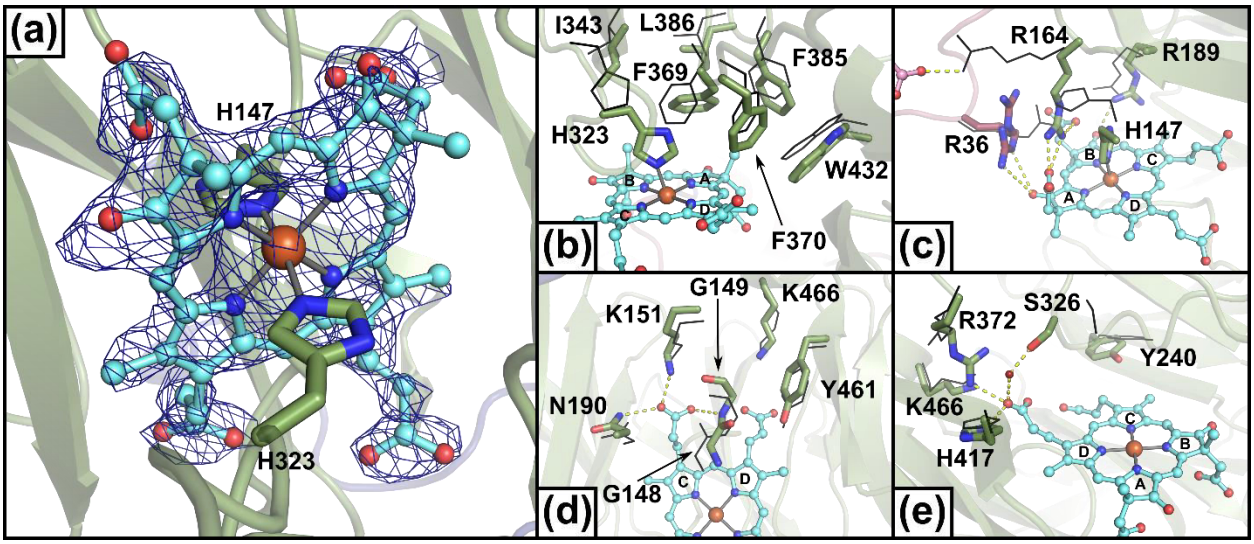
(a)
H147
H323
(b)
I343
L386
F385
F369
H323
W432
F370
(c)
R164
R189
R36
H147
(d)
G149
K466
K151
Y461
N190
G148
(e)
S326
R372
Y240
K466
H417

Figure 5

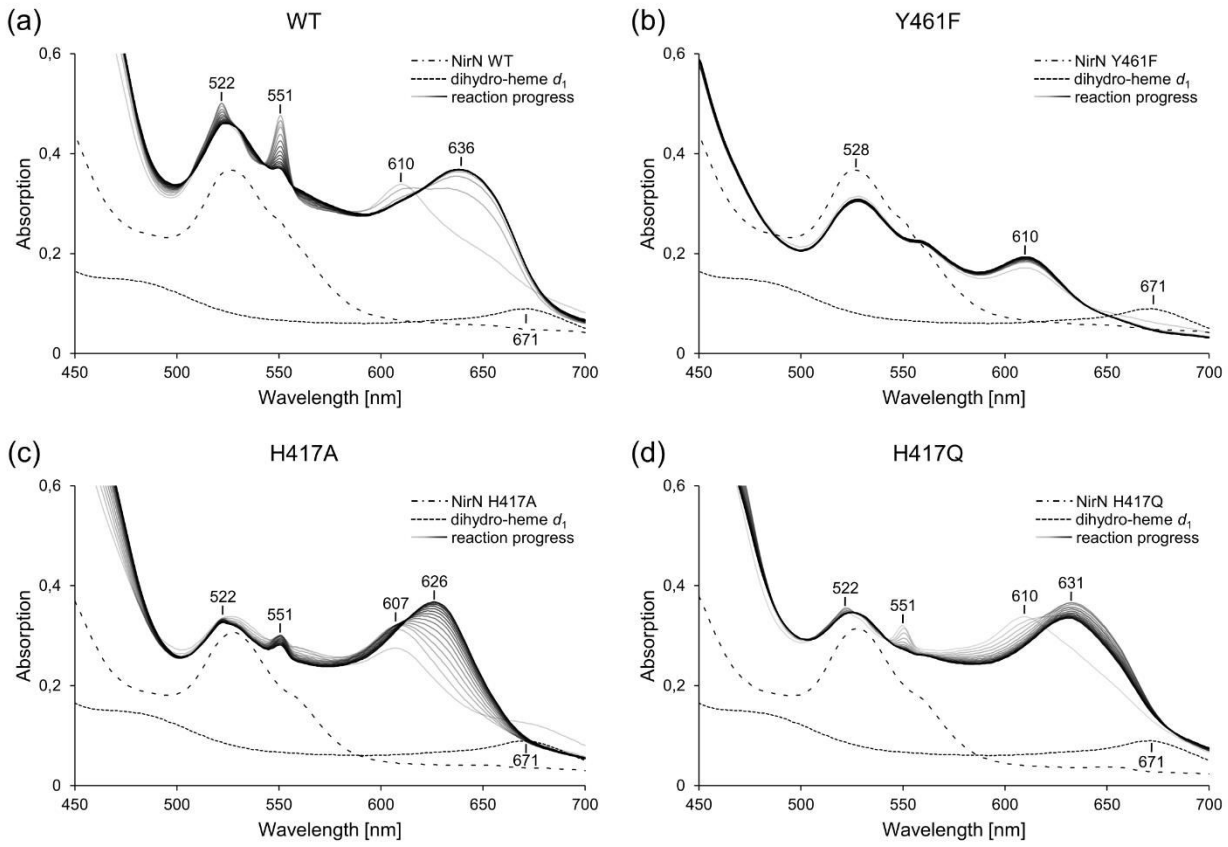
(a)
WT
NirN WT
dihydro-heme d_1
reaction progress
522
551
610
636
671
Absorption
Wavelength [nm]
(b)
Y461F
NirN Y461F
528
610
671
(c)
H417A
NirN H417A
522
551
607
626
671
(d)
H417Q
NirN H417Q
522
551
610
631
671

Figure 6

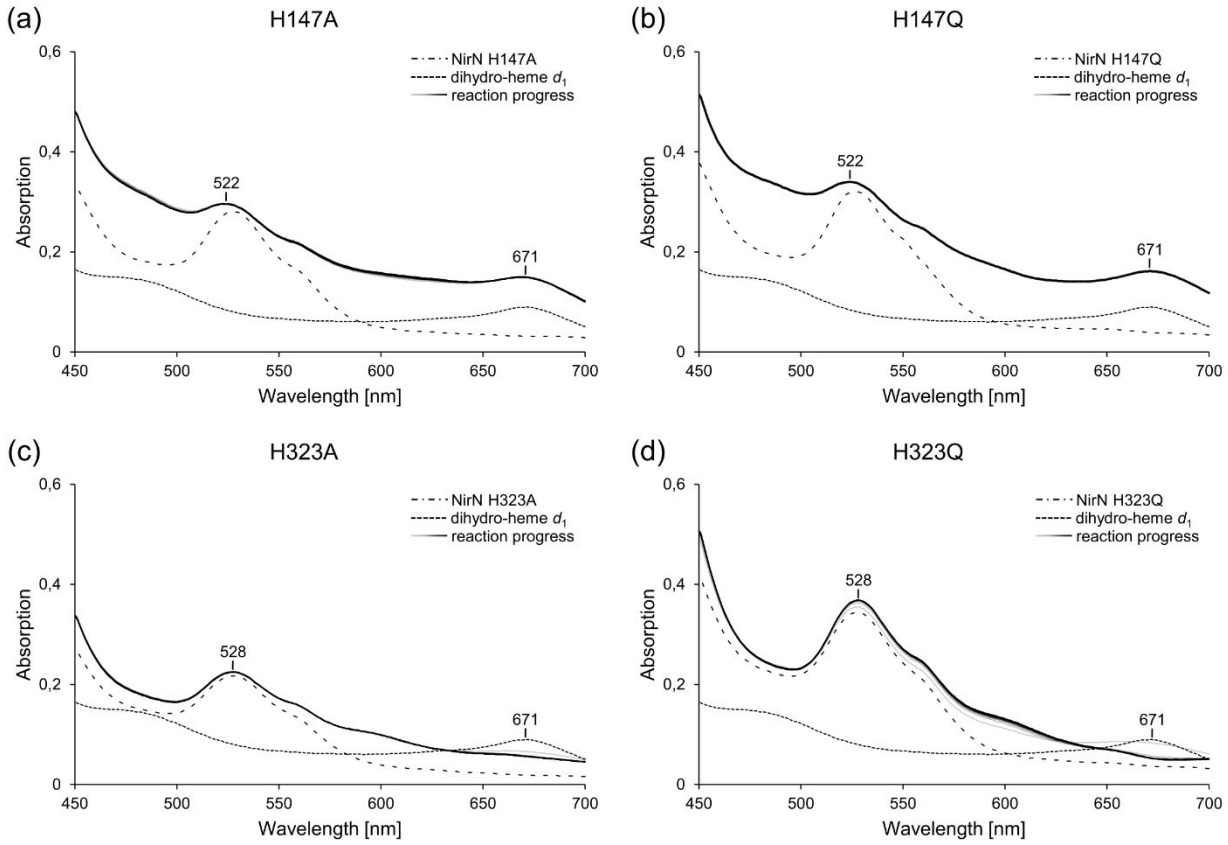
(a)
H147A
NirN H147A
dihydro-heme d_1
reaction progress
522
671
Absorption
Wavelength [nm]
(b)
H147Q
NirN H147Q
dihydro-heme d_1
reaction progress
522
671
Absorption
Wavelength [nm]
(c)
H323A
NirN H323A
dihydro-heme d_1
reaction progress
528
671
Absorption
Wavelength [nm]
(d)
H323Q
NirN H323Q
dihydro-heme d_1
reaction progress
528
671
Absorption
Wavelength [nm]